Helical Liquid Flow on a Vertical Cylinder and Its Application to Gas Absorption

Naoya Komae, Yuki Sato, and Yasuhiko H. Mori
Dept. of Mechanical Engineering, Keio University, Kohoku-ku, Yokohama 223–8522, Japan

DOI 10.1002/aic.14079
Published online March 14, 2013 in Wiley Online Library (wileyonlinelibrary.com)

An experimental examination of a novel device for enhancing the gas absorption into an aqueous absorbent flowing down the outer wall of a vertical cylinder was reported. This device utilizes flexible strings tightly wound around the cylinder, taking the form of a multiple helix. The absorbent flows along parallel channels partitioned by the strings, maintaining mutual contact with the surrounding gas for a longer time than it would when it flows down the same cylinder wall in the absence of such strings. Both flow-observation experiments and absorption experiments using water as the absorbent flowing along a single helical channel and carbon dioxide as the gas to be absorbed were carried out. The effectiveness of the helical-flow device for promoting the absorption was recognized at water flow rates high enough to induce an oscillatory flow mode accompanied by periodical liquid−gas interface deformation. © 2013 American Institute of Chemical Engineers *AIChE J*, 59: 3109–3118, 2013
Keywords: gas absorption, gas−liquid contactor, CO_2 separation, mass transfer, mass-transfer equipment

Introduction

There are various equipment designs for gas−liquid contactors applicable for industrial gas-absorption (or wet scrubbing) processes, the importance of which is currently increasing due to the increasing need for removing greenhouse gases (typically carbon dioxide) from industrial exhaust gases. Many of the existing designs were devised to make liquid absorbents take the form of thin films flowing down the vertical walls of tower-type contactors or some packing materials such as Raschig rings or structured packings made of thin corrugated plates.[1,2] Such packing materials may be replaced by bundles of vertically oriented straight wires.[3,4] Obviously, these packing materials or structures installed inside the contactors significantly extend the liquid–gas interfacial area and possibly promote the internal mixing of both the liquid and the gas phases, thereby promoting the mass and/or heat transfer between these phases. On the other hand, they provide some drawbacks such as an increased pressure loss in the gas flow, difficulty in cleaning and maintenance of the contactors, and higher costs for constructing and maintaining the contactors. As a result, wetted-wall columns having no internal structure are widely used in industries due to their durability for treating, for example, a flue gas containing various pollutants often including particulate matter. Although not yet put to practical use, some research efforts have been devoted to improving the mass-transfer or gas-absorption performance of wetted-wall columns by applying passive or active means for inducing turbulence, helical motion, or surface waves in the liquid films flowing down the column walls. For example, Broniarz-Press[5] reported experimental examinations of the effects of several types of helical roughnesses formed on the outside surfaces of vertical cylinders on each of which water flowed down while in contact with a counter flow of carbon dioxide (CO_2) gas in a coaxial annular space. Hijikata et al.[6] and Nosoko and his coworkers[7,8] investigated the surface waves generated by acoustic oscillators on the water films flowing down vertical walls (the outside surface of a vertical cylinder, a vertical flat plate, and the inside surface of a vertical cylinder) and their effects on the absorption of CO_2 or oxygen (O_2) into the films. Despite its significant effect on gas absorption observed in these laboratory studies, such an active wave-inducing technique is not necessarily suitable for large-scale industrial gas-processing equipment in which the construction cost and the structural simplicity leading to a higher durability and easier maintenance are of major concern.

This study attempted to examine a novel passive technique for possibly improving the gas-absorption performance of wetted-wall columns. The technique requires only a simple handicraft processing of the column walls that may be applied not only to equipment to be newly constructed but also to existing equipment. The basic idea of this technique is schematically illustrated in Figure 1. Either the outside or the inside surface of a vertical cylinder on which a liquid absorbent is to flow down is divided into helical channels by flexible strings that tightly wind around a cylinder [illustration (a) in Figure 1] or are stuck on the inside surface of a hollow cylinder [illustration (b) in Figure 1]. The strings are geometrically congruent and axially aligned at uniform intervals such that the channels each bordered by two neighboring strings have the same width. Although only three strings (and hence three channels) are illustrated in Figure 1 for

Correspondence concerning this article should be addressed to Y. H. Mori at yhmori@mech.keio.ac.jp.
Current address of N. Komae: Misato Plant, Eisai Co., Ltd., Misato-cho, Kodama-gun, Saitama Prefecture 367-0198, Japan.

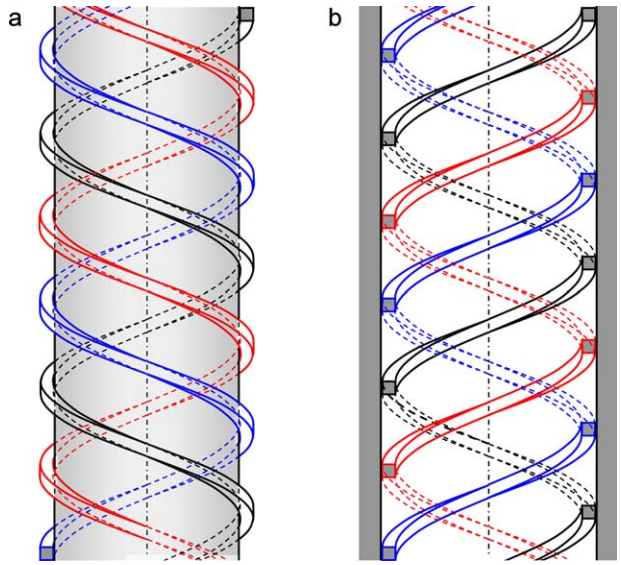

Figure 1. A multiple helix consisting of three strings in rectangular cross section (each discriminated from the others by color) tightly winding around a cylinder, (a), or stuck on the inside surface of a hollow cylinder, (b).

[Color figure can be viewed in the online issue, which is available at wileyonlinelibrary.com.]

graphic simplicity, the number of strings should be further increased for practical use to reduce W, the width of each channel (defined as the gap between two neighboring strings as illustrated in Figure 2), such that a rivulet of the liquid absorbent is stably held inside the channel by the gas−liquid interfacial tension, γ, working at the rivulet surface bridging the two neighboring strings. This means that W cannot significantly exceed the so-called capillary length a defined as follows

$$a^2 = \frac{2\gamma}{(\rho_L - \rho_G)g} \tag{1}$$

where ρ_L, ρ_G, and g denote the liquid-absorbent density, gas density, and the acceleration due to gravity, respectively. To be more specific, the suitable range of W should depend not only on a but also on the geometry and dimensions of the string cross sections (w_1 and w_2 indicated in Figure 2 for strings having rectangular cross sections), the wettability of the strings with the liquid absorbent, the tilt angle of the strings measured from the horizontal (θ indicated in Figure 2), the diameter of the cylinder (D indicated in Figure 2), and the liquid-absorbent flow rate through each channel. The string cross sections may be different from rectangular; they may be circular, triangular, or trapezoidal. It is desirable that the string material should be moderately wettable with the absorbent to provide a sufficiently large capillary force with which the liquid rivulet clings to the strings. Highly liquid-repellent strings will only slightly exert such a capillary force on the rivulet. On the contrary, highly wettable strings will not work as effective barriers against the spreading of the absorbent from one channel to the neighboring channels, and will possibly allow a part of the absorbent to flow straight down the cylinder by crossing the strings thereby making a shorter contact time with the gas phase than it would make if it flowed along the helical channels. Although we used rubber strings in this study for experimental convenience, they may be replaced by helical metal ribbons welded onto the cylinder surface or by helical ridges generated by machining of the cylinder itself.

The primary point of the helical-string device described above is to extend the path of the liquid absorbent during its passage through a given wetted-wall-type gas−liquid contactor. If the effective height of the contactor is H, the path of each helical channel is extended to H $(\sin\theta)^{-1}$, which should lead to a longer gas−liquid contact time inside the contactor and possibly a higher efficiency of the contactor. Regarding this point, the helical-string device dealt with in this study should be discriminated from such helical roughness elements as those studied by Broniarz-Press,[5] which were entirely covered with falling liquid films and played the role of turbulence promoters, instead of helical-flow conduits.

In this study, we first performed water-flow observation experiments using a single helical channel formed on the outside surface of a vertical cylinder exposed to laboratory air, then performed CO_2-to-water absorption experiments using annular contactors each composed of an inner cylinder equipped with a single helical channel and a coaxial outer cylinder confining the CO_2 gas flowing upward. The gas-absorption performance of such test contactors depending on the helical-channel geometry as well as the water flow rate through the channel was examined, and the performance of hypothetical contactors equipped with multiple helical channels was estimated.

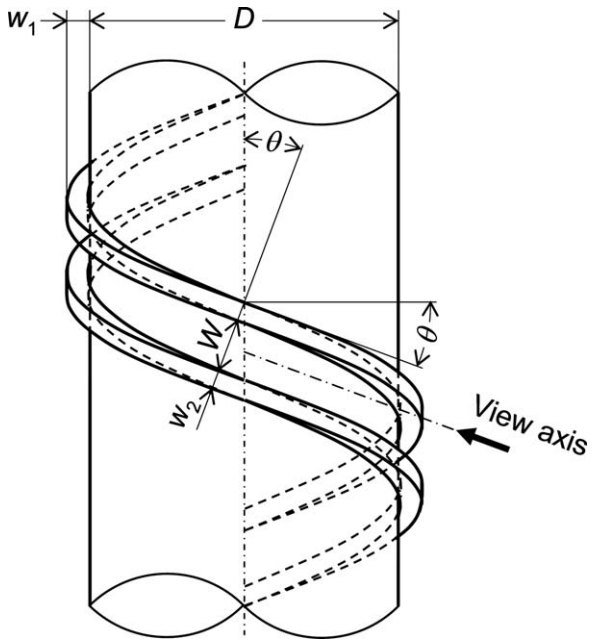

Figure 2. Schematic illustration of the string-geometry parameters.

The parameters are D, the diameter of the cylinder around which the strings are wound; w_1, the string thickness measured in the radial direction; w_2, the string thickness measured in the direction perpendicular to that for measuring w_1; W, the width of the space between the neighboring strings; and θ, the tilt angle of the strings measured from the horizontal. The view axis relevant to the microscopic observation of the liquid-film flow along the helical channel between the strings is also indicated.

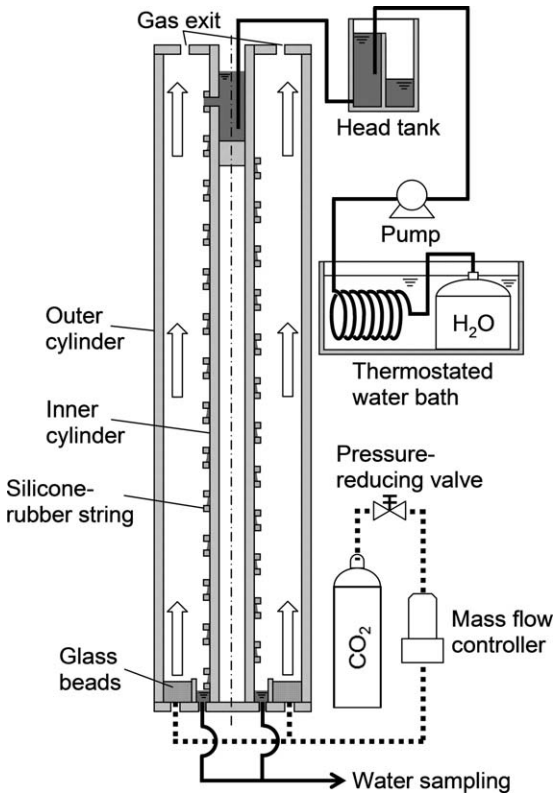

Figure 3. Schematic illustration of the experimental setup.

The setup used in the gas-absorption experiments is illustrated here. The outer PMMA cylinder and the CO_2 supply assembly were not installed in the flow-observation experiments.

Description of Experiments

Apparatus and procedure

Figure 3 schematically illustrates the experimental setup used for the gas-absorption experiments. The major portion of this setup was a 1-m height annular gas−liquid contactor composed of coaxial poly(methyl methacrylate) (PMMA) cylinders. The inner cylinder, 40 or 60 mm in outside diameter, was wrapped with a pair of silicone-rubber strings, 3-mm square in cross section, that formed a single helical channel having a constant width, $W = 4$ mm. Specifications of the four different types of inner cylinders alternatively used in this study are listed in Table 1. The outer cylinder had 144-mm inside diameter. The annular space between the two cylinders served as the flue through which CO_2 gas flowed upward, while in contact with the water which was flowing down the helical channel winding around the inner cylinder. The bottom of this annular space contained a 40-mm height bed of 4-mm dia. glass beads to make the CO_2 gas flow at the inlet of the space circumferentially and radially uniform. The space was capped by an annular PMMA plate on which 16 10-mm dia. vent holes were drilled at even circumferential intervals. These holes allowed the CO_2 gas to flow out of the annular space without inducing a significant distortion of the gas flow field near the top end of the space. Water used as the absorbent for CO_2 was supplied to the top of the helical channel at a constant rate. The top portion, 100 mm in height, of the inner cylinder was tightly wrapped with a poly(ethylene terephthalate) sheet such that the helical channel within this portion became a closed rectangular conduit. Hence, the actual gas−liquid contact section extended 800 mm downward from the height 100-mm below the top edge of the cylinder. Water having flowed down this gas−liquid contact section was drained from the helical channel through a port located at the bottom of the annular space of the contactor.

Three auxiliary assemblies were connected to the gas−liquid contactor. One of them was for supplying water as the absorbent to the top of the contactor. This assembly consisted of a water reservoir and a coil heat exchanger both immersed in a water bath temperature-controlled at 25°C, a tubing pump (Masterflex® model HV-07523-60) and a head tank. The rate of the water supply to the contactor was controlled by varying the elevation of the head tank, which was initially calibrated to the water flow rate. The second assembly was for supplying CO_2 gas to the bottom of the contactor. It consisted of a liquefied CO_2 cylinder, a pressure-reducing valve and a mass-flow controller (Estec SEC-E50/PAC-D2) connected in series. The rate of CO_2 gas supply was controlled so that the superficial velocity of the gas flowing upward through the annular space of the contactor was limited to 1.1 mm/s to prevent the gas flow from exerting any appreciable hydrodynamic effect on the water flow along the helical channel. The third assembly was for draining the water having flowed down the helical channel out of the gas−liquid contactor. This assembly connecting the bottom of the gas−liquid contactor and a reservoir for collecting the water was operated so that it was always filled with the water and no gas bubble was dragged into it. A sampling port was attached to the conduit connecting the contactor and the reservoir for obtaining water samples. These samples were analyzed later using a total organic carbon analyzer (Shimadzu TOC-500) to determine the concentrations of CO_2 dissolved in them.

The experimental setup used for the water-flow observation was somewhat different from the one described above. Neither the outer cylinder of the gas−liquid contactor nor the CO_2 supply assembly was used such that water flowed through the helical channel on the inner cylinder while being in direct contact with the laboratory air temperature-controlled at 25 ± 1°C. Also, the water draining assembly was replaced by a simple conduit that directly connected the drain at the bottom of the gas−liquid contactor to the water reservoir immersed in the thermostated bath to make a closed loop for water circulation via the helical channel. Visual observation was carried out using a digital microscope (Keyence VH-5000) connected to a video deck (Sony WV-DR5) and a personal computer along the view axis indicated in Figure 2 to obtain peripheral views of the helical channel holding a water flow as stills or motion pictures.

Table 1. Specifications of Four Types of Test Cylinders Each Entwined with a Pair of Silicone-Rubber Strings Forming a Helical Channel for Water Flow

Type	D (mm)[a]	θ (°)[a]	w_1 (mm)[a,b]	w_2 (mm)[a,b]
A	40	30	2.7	2.8
B	40	45	2.65	2.8
C	40	60	2.35	2.55
D	60	45	2.65	2.8

[a]As for the notations D, θ, w_1, and w_2, consult Figures 2 and 4.
[b]The values of w_1 and w_2 actually observed on the test cylinders were different from the nominal string thickness, 3 mm, depending on the tension loaded on the strings when they were wound around each cylinder.

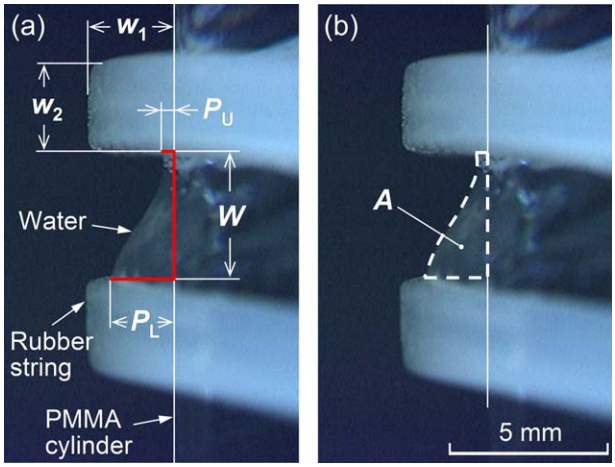

Figure 4. Measurements of the wetted perimeter in a helical channel and the cross-sectional area of the water flow along the channel.

The cross-sectional image of the channel shown here was viewed along the "view axis" indicated in Figure 2. The type A test cylinder was used. The water flow rate $\dot{V}$ was 135 cm^3/min. In (a), the wetted perimeter P is traced by the red line. P is given as the sum of P_U, the wetted radial length on the upper string, P_L, the wetted radial length on the lower string, and W, the width of the channel between the two strings. In (b), the cross-sectional area of the water flow, A, is enclosed by thick dashed lines. [Color figure can be viewed in the online issue, which is available at wileyonlinelibrary.com.]

Materials

Throughout the flow-observation and gas-absorption experiments, water deionized and distilled in our laboratory was exclusively used as the liquid that flowed down the helical channels. Liquefied CO_2 of 99.9% (molar basis) certified purity (supplied by Toyoko Kagaku, Kawasaki, Kanagawa Prefecture, Japan) was used to generate the CO_2 gas for the gas-absorption experiments.

Data processing

Based on the videographs obtained during the flow-observation experiments and using an image-analysis software (LIA for Win32, ver. 0376β1), we determined several geometric quantities such as those indicated in Figure 4—that is, P_U, the wetted width on the upper string surface; P_L, the wetted width on the lower string surface; P, the wetted perimeter of the channel given by $P_U + W + P_L$; and A, the cross-sectional area of the water rivulet confined in the channel. For each experimental condition, 5–15 still pictures successively taken at 1-s intervals were used to measure the instantaneous values of these quantities. The arithmetic mean of these values of each quantity was determined as its representative value. In an oscillatory flow regime, 15 pictures were used to determine the representative values of the quantities with sufficient statistical reliability. Based on these quantities, we derived the following quantities characterizing the water flow through each helical channel

$$\delta = A/W \tag{2}$$

$$\bar{u} = \dot{V}/A \tag{3}$$

$$\tau = L/\bar{u} \tag{4}$$

$$Re_f = \frac{4\dot{V}}{\nu P} \tag{5}$$

where $\dot{V}$, ν, and L denote the volume flow rate of water, the kinematic viscosity of water, and the axial length of the helical channel corresponding to the 800-mm height gas–liquid contact section, respectively. Hence, δ, $\bar{u}$, τ, and Re_f mean the thickness of the water rivulet averaged over the channel width, the water-flow velocity averaged over the cross section of the rivulet, the mean transit time of the water flow through the channel, and the Reynolds number for the water flow through the channel, respectively.

The raw data obtained in the gas-absorption experiments were the values of the carbon contents of the water samples. Assuming that such carbon contents were entirely due to the dissolved CO_2, we evaluated C, the mass concentration of CO_2 in each sample. In each experiment, we repeated the carbon-content measurements 8–24 times with separate water samples obtained at 1- to 5-min intervals and determined the arithmetic mean of the C values for these samples as the representative C value for the operational conditions specified in this experiment. In the following description, the C values relevant to the samples taken from the water flowing out the contactor at the bottom are denoted by C_{bot}, while those relevant to the samples taken from the water flowing into the contactor at the top are denoted by C_{top}. The solubility of CO_2 in water under a CO_2-gas pressure of 0.1013 MPa is denoted by C_{sat}. Based on these specific C values, we calculated $\bar{k}_L$, the liquid-side mass-transfer coefficient averaged over the nominal gas–liquid interfacial area given by WL, and E, the liquid-side absorption efficiency, as follows

$$\bar{k}_L = \frac{\dot{V}}{WL} ln\left(\frac{C_{sat} - C_{top}}{C_{sat} - C_{bot}}\right) \tag{6}$$

$$E = \frac{C_{bot} - C_{top}}{C_{sat} - C_{top}} \tag{7}$$

The derivation of Eq. 6 is shown in Appendix A. The value of C_{sat} was determined using the Henry's law constant for a CO_2–water system, k_H, given by the following van't Hoff equation

$$k_H = k_{H0} \exp\left[\gamma\left(\frac{1}{T} - \frac{1}{T_0}\right)\right] \tag{8}$$

where T denotes the absolute temperature of the sampled water ($\approx$298 K), and the other quantities on the right-hand side were cited from the literature[9] as follows: k_{H0} = 0.35 mol/(kg MPa), γ = 2400 K, and T_0 = 298.15 K.

Results and Discussion

Helical-flow characteristics

Our visual observation of the water flow using the four types of test cylinders (Table 1) revealed that stable flow occupying the full width W of each helical channel (see Figure 4) is available only in a specified flow-rate range. If the flow rate was too low, water did not completely wet the cylinder surface between the two rubber strings and formed an unstable thread-like rivulet trickling along the helical channel. On the contrary, excessively high flow rates caused scattering of droplets from the surface of the water rivulet and even detachment of the rivulet itself from the channel. Due to the difficulty of accurately maintaining very low flow rates in our experimental system, we did not attempt to determine the minimum flow rate for the stable flow regime. Instead, we confirmed that the flow rate, $\dot{V}$ = 42 cm^3/min, is

Table 2. The Critical Flow Rates $\dot{V}_{cr}$ for the Occurrence of Oscillatory Motions of the Water Rivulets Flowing on the Test Cylinders and the Maximum Flow Rates $\dot{V}_{max}$ for the Stable Helical Flows on These Cylinders Free from Any Disintegration of the Rivulets

Test Cylinder	$\dot{V}_{cr}$ (cm^3/min)	$\dot{V}_{max}$ (cm^3/min)
A	180	186
B	179	233
C	222	331
D	254	333

sufficient to sustain a stable flow on every type of test cylinder. The maximum flow rate for the stable flow mode, $\dot{V}_{max}$, was experimentally determined for each type of test cylinder and is indicated in Table 2. The determined $\dot{V}_{max}$ values for the four types of test cylinders indicated that the smaller the cylinder diameter D or the channel tilt angle θ, the lower the relevant value of $\dot{V}_{max}$. This observation is in qualitative agreement with our mechanistic understanding that the centrifugal force working on a thin water layer ($\delta << D$) flowing along a helical channel at the axial velocity of u is proportional to $(u\cos\theta)^2/D$. Although we made no experiment with any helical channel stuck on the inside surface of a hollow cylinders (Figure 1b), it is reasonable to assume that there will be no centrifugal-force-dependent flow-rate limit for the stable flow regime in the case of such an internal helical flow. Presumably, the upper limit of the flow rate in that case is related to the flooding of the channel by a gravity-driven water flow.

The stable flow regime described above may be classified into two subregimes limited by a critical flow rate $\dot{V}_{cr}$. At flow rates below $\dot{V}_{cr}$, the geometry of such cross sections of each water rivulet as the one shown in Figure 4 hardly changed with time. As $\dot{V}$ exceeded $\dot{V}_{cr}$, the geometry of each cross section exhibited a nearly periodic oscillatory motion. A typical sequence of such an oscillatory motion is shown in Figure 5. The $\dot{V}_{cr}$ values for the four types of test cylinders are listed, together with the corresponding $\dot{V}_{max}$ values, in Table 2.

Figure 6 shows how the cross-section geometry of the water rivulets flowing along the helical channels vary depending on $\dot{V}$, focusing on the geometry-representing quantities indicated in Figure 4—that is, P_U, P_L, P ($=P_U+P_L+W$), and A. Two specific flow rates, $\dot{V}_{cr}$ and $\dot{V}_t$, are marked on the abscissa, where $\dot{V}_t$ is the flow rate corresponding to a specific Reynolds number, $Re_f = 1500$, which is known to be the critical Reynolds number for the transition of two-dimensional (2-D) film flows from the laminar to turbulent regime.[10,11] It appears from Figure 6 that the tendency of monotonic increases in P_U, P_L, P, and A with an increase in $\dot{V}$ observed in the $\dot{V}$ range up to $\sim\dot{V}_t$ eased or almost vanished as $\dot{V}$ exceeded $\sim\dot{V}_t$. As $\dot{V}$ exceeded $\dot{V}_{cr}$, P_U, P_L, P, and A again tended to increase. The oscillatory motion of water rivulets characterizing this $\dot{V}$ range caused significant fluctuations in P_U, P_L, P, and A, which are reflected by the relatively long error bars (indicating the relevant standard deviations) accompanying the data points in this $\dot{V}$ range.

Figures 7 and 8 show the data of the water-rivulet thickness δ deduced from those of A via Eq. 2 and the estimates of τ, the mean transit time of the water flow through each helical channel, given by Eq. 4, respectively. These δ and τ values are plotted vs. Re_f, instead of $\dot{V}$, for the convenience of comparing them with the corresponding values for 2-D water films vertically falling the same height as that of the helical channels ($H = 80$ cm) in a wetted-wall column. The procedure for calculating the film-thickness δ and transit timeτ for the wetted-wall column is described in Appendix B. Figure 7 reveals that the water rivulets flowing through the helical channels on the 40-mm dia. cylinders (types A−C) were thicker than those flowing through the channel on the 60-mm dia. cylinder (type D) and that all of them were significantly thicker than the 2-D water films falling down the plain wall of a wetted-wall column if compared on a Re_f basis. This nature of the helical channel flows seems to be unfavorable for their application to gas-absorption processes. On the other hand, Figure 8 indicates that, as expected, the helical channels yielded significantly longer transit times than that available with the wetted-wall column at any level of Re_f within the range of our flow-observation experiments. Comparing the τ vs. Re_f plots for the four test cylinders, we can readily confirm that the smaller the tilt angle θ of the channel, the longer the transit time τ was extended.

Absorption performance

Figure 9 summarizes the results of gas-absorption experiments using the four types of test cylinders. For any type of test cylinder, we observed a monotonic increase in the average mass-transfer coefficient, $\bar{k}_L$, with an increase in the water flow rate $\dot{V}$. It is obvious that, as $\dot{V}$ approached or exceeded $\dot{V}_{cr}$, $\bar{k}_L$ tended to sharply rise. The absorption efficiency E decreased with an increasing $\dot{V}$ in a region below $\dot{V}_t$, but simultaneously exhibited an upturn at a certain flow rate in the range between $\dot{V}_t$ and $\dot{V}_{cr}$ as $\bar{k}_L$ started to sharply rise. These observations indicate that the CO_2 absorption into the water rivulets strongly depended on the hydrodynamic turbulence induced in them and, presumably to an even higher extent, their oscillatory bulk motions such as the one demonstrated in Figure 5.

Figure 10 compares, in the form of $\bar{k}_L$ and E vs. Re_f diagrams, the gas-absorption performance observed with the four types of test cylinders to the corresponding estimates

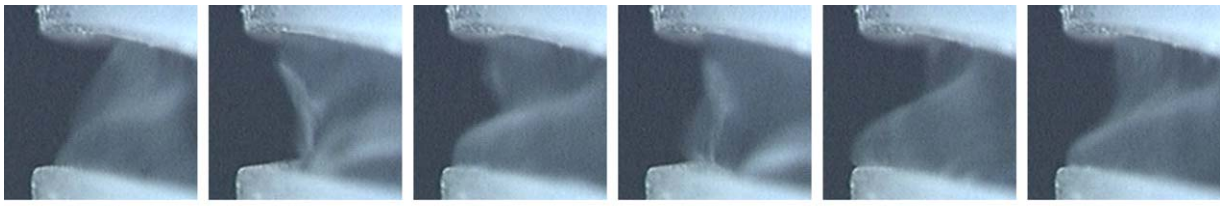

Figure 5. Oscillatory water flow observed on the type *B* cylinder.

$\dot{V} = 179$ cm^3/min, $Re_f = 1776$. t denotes the lapse of time from an arbitrarily selected instant when the leftmost image was taken.

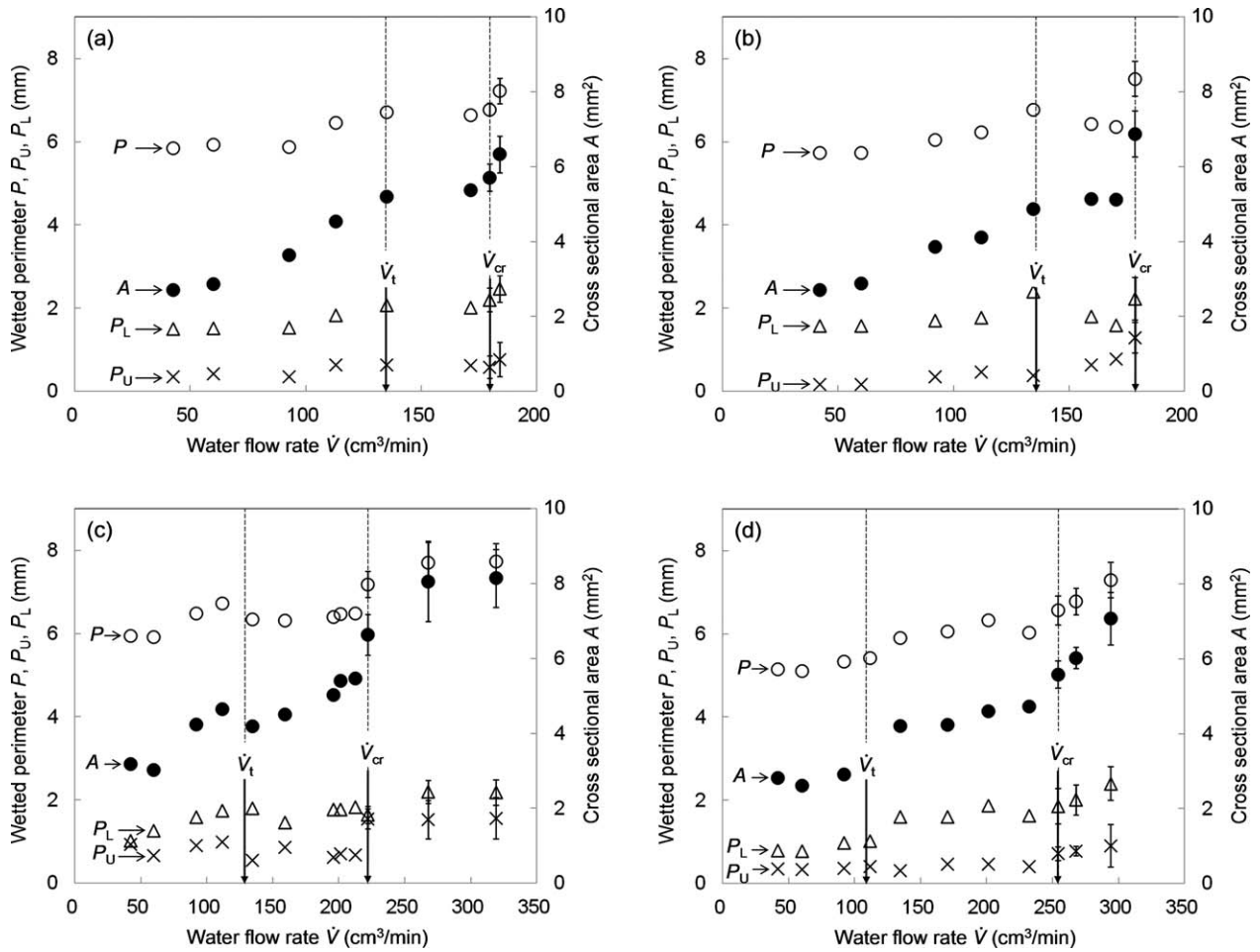

Figure 6. Wetted perimeter and cross-sectional area of water flow vs. water flow rate.

As for the definitions of P, P_U, PL, and A, consult Figure 4. $\dot{V}_t$ denotes the water flow rate corresponding to the critical Reynolds number, $Re_f = 1500$, known as the condition for the laminar-to-turbulent flow transition for planar film flows. $\dot{V}_{cr}$ denotes the critical flow rate beyond which the water flow exhibits such an oscillatory motion as that shown in Figure 5. The experimental data obtained for the A–D test cylinders are plotted on separate graphs (a)–(d), respectively. Each data-point symbol indicates the arithmetic mean of 5–15 data points based on videographic still images obtained at 1-s intervals. The error bar laid on the data-point symbol indicates the magnitude of the standard deviation of the data points. Error bars not exceeding the linear dimension of the data-point symbols are omitted.

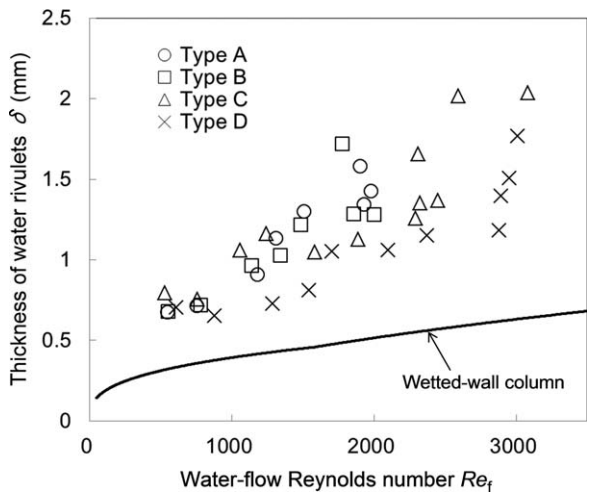

Figure 7. Thickness of water rivulets flowing through helical channels.

The experimental data obtained for the four types of test cylinders are compared with the estimated thickness of a 2-D water film flowing down the vertical plain wall of a conventional wetted-wall column.

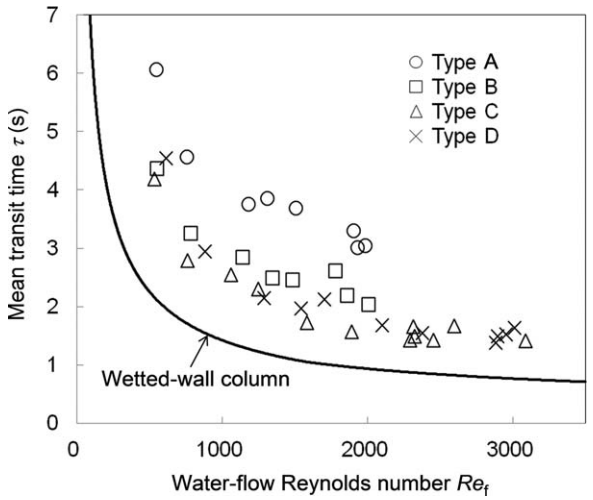

Figure 8. Mean transit time for water passing through each helical channel.

The experimental data obtained for the four types of 80-cm height test cylinders are compared with the estimated transit time for water flowing down a conventional 80-cm height wetted-wall column.

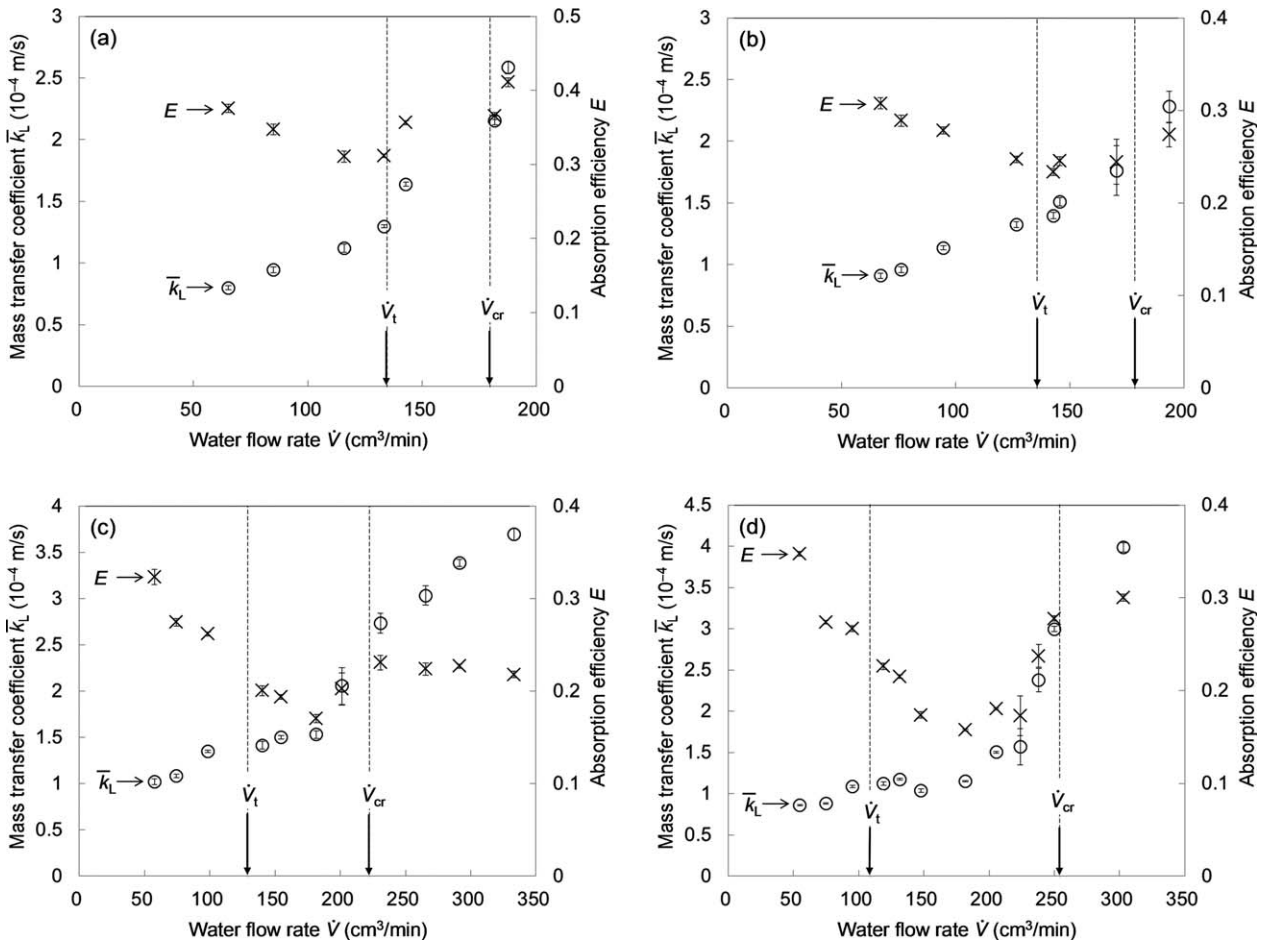

Figure 9. Average mass-transfer coefficient and absorption efficiency vs. water flow rate.

The experimental data obtained for the A–D test cylinders are plotted on separate graphs (a)–(d), respectively. Each data-point symbol indicates the arithmetic mean of 8−24 CO_2-in-water concentration data points obtained by repeated measurements using a TOC analyzer. The error bar laid on the data-point symbol indicates the magnitude of the standard deviation of the data points. Error bars not exceeding the linear dimension of the data-point symbols are omitted.

for a conventional 80-cm height wetted-wall column. The procedure that we used to estimate the $\bar{k}_L - Re_f$ and $E - Re_f$ relations for the wetted-wall column is described in Appendix C. Figure 10 indicates that, regarding $\bar{k}_L$, test cylinders A−C ($D = 40$ mm) surpassed the wetted-wall column whenever Re_f exceeded ~1500 (or $\dot{V}$ exceeded $\sim\dot{V}_t$). Test cylinder D ($D = 60$ mm) did not exceed the wetted-wall column until Re_f exceeded ~2700 (or $\dot{V}$ exceeded $\sim\dot{V}_{cr}$). With respect to E, the advantage of the helical-flow cylinders is more limited. A substantial advantage over the wetted-wall column was observed only with test cylinder A in a Re_f range above ~1300 and with test cylinder D in a Re_f range above ~2700. This fact is ascribed to the helical-flow rivulets being much thicker than the 2-D film vertically flowing down in the wetted-wall column under each given Re_f condition (see Figure 7). The larger rivulet thickness (i.e., the smaller gas−liquid interfacial area per unit liquid volume) must have diminished the effect of the higher $\bar{k}_L$ on E.

The comparison between the helical-flow cylinders and a conventional wetted-wall column equal in height as presented in Figure 10 may be instrumental to our understanding of the general characteristics of the gas absorption into the helical channel flows. It should be noted, however, that this comparison does not directly lead to a comparative evaluation of a helical-channel column, an annular column coaxially holding an inner cylinder the surface of which is completely covered by helical channels as illustrated in Figure 1a, as a substitute for a wetted-wall column. Such an evaluation should be based on the E value available when the absorbent (water) is supplied to the helical-channel column at the same flow rate as that supplied to a wetted-wall column having the same height, H, and same surface area to be swept by the gas flow, πDH, as those of the helical-channel column. It is necessary to take into account that a finite fraction [$= w_2/(W + w_2)$] of the surface area of the helical-channel column is covered by the channel-separating strings, instead of the absorbent, and hence reduces the effective gas−liquid contact area as compared to the conventional wetted-wall column. We assumed four 80-cm height helical-channel columns each holding a 40- or 60-mm dia. inner cylinder covered by multiple helical channels that are geometrically identical to the single channel installed on the type A, B, C, or D test cylinder. We call the column equipped with the channels identical to that on the type A test cylinder "column A," and so forth. The E vs. $\dot{V}$ data obtained using the type A (B, C, or D) test cylinder can be used to predict those for column A (B, C, or D) just by multiplying $\dot{V}$ for the test cylinder by N, the number of helical channels formed on the inner cylinder of the column. Based on a simple geometrical consideration, we can determine N as follows

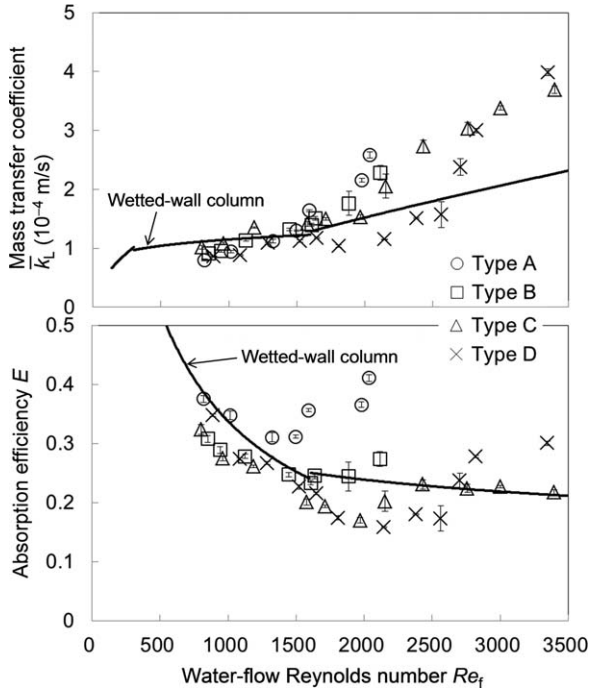

Figure 10. Average mass-transfer coefficient and absorption efficiency vs. water-flow Reynolds number.

The experimental data obtained for the four types of test cylinders are compared with the corresponding estimates for water flowing down a conventional 80-cm height wetted-wall column.

$$N = \frac{\pi D \sin\theta}{W + w_2} \tag{9}$$

For actually constructing a helical-channel column, we must adjust the geometrical column-design parameters (D, θ, w_2, and W) such that N becomes a positive integer. For the present purpose of evaluating the performance of "hypothetical" helical-channel columns, however, we used the noninteger N numbers deduced by simply substituting the parameter values given in Table 1 into Eq. 9. As for w_2, we also examined a hypothetical case in which w_2 is reduced to 1 mm without changing W, thereby resulting in an increase in N. The values of N thus determined for each of the four helical-channel columns, A–D, are summarized in Table 3. The E vs. $\dot{V}$ data for these columns are plotted in Figure 11 together with the E vs. $\dot{V}$ relations estimated for a corresponding wetted-wall column having a wetted perimeter equal to the circumference of a 40- or 60-mm dia. cylinder (see Appendix C for the details of the estimation about the wetted-wall column). This figure indicates that the advantage

Table 3. Specifications of the Four Hypothetical Helical-Channel Columns ($H = 80$ cm) Assumed for the Purpose of Gas-Absorption Performance Evaluation

			Number of Channels N	
Column	D (mm)	θ (°)	w_2 Indicated in Table 1	$w_2 = 1$ mm
A	40	30	9.2	12.6
B	40	45	13.1	17.8
C	40	60	16.6	21.8
D	60	45	19.6	26.7

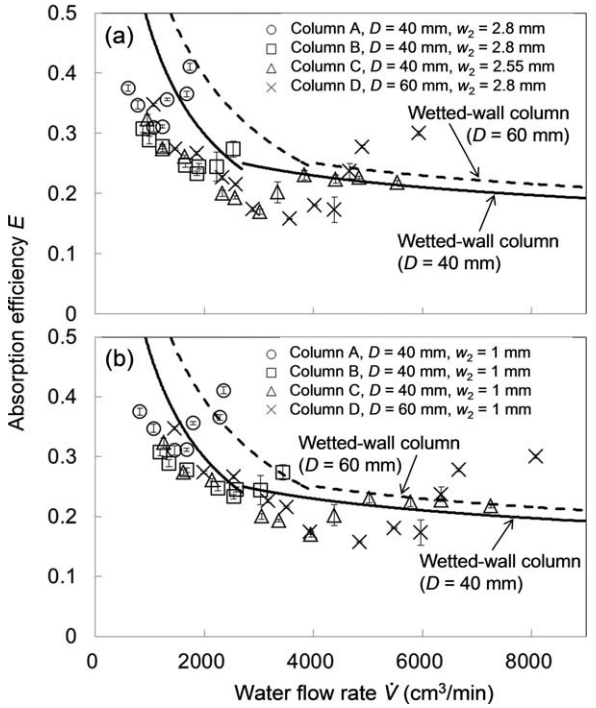

Figure 11. Absorption efficiency vs. water flow rate—comparison between virtual helical-channel columns and a conventional wetted-wall column having the same height and surface area.

In (a), the number of helical channels to be formed on each 40- or 60-mm dia. cylinder were determined based on the w_2 values actually measured in the experiments (see Table 1). In (b), w_2 was assumed to be reduced to 1 mm, resulting in a higher number of channels and thereby a higher water flow rate.

of the helical-channel columns over the corresponding wetted-wall column is unexpectedly limited. If the same strings that we used in preparing the test cylinders are used in constructing the helical-channel columns, we can expect only a ~30% increase in E at best in a narrow $\dot{V}$ range around or above $\dot{V}_{cr}$ (Figure 11a). The advantage of the helical-channel columns can be moderately improved by reducing w_2, the width of the strings or the helical ridges machined on the inner cylinder surfaces, thereby increasing $\dot{V}$ without changing E (Figure 11b).

Concluding Remarks

A technical idea for inducing a helical flow of a liquid on the outside or inside wall of a vertical cylinder thereby promoting the gas absorption into the liquid has been proposed and examined based on small-scale laboratory experiments. The idea was to form fin-like ridges aligned in the form of a multiple helix on the cylinder wall and to make the liquid flow along the helical channels partitioned by the ridges. The ridges may be formed by, for example, winding strings around the cylinder or by direct machining of the cylinder wall. Due to a technical reason about our self-building of the experimental apparatus, the experiments were performed exclusively for the case of a liquid flow on the outside wall of a vertical cylinder, in which the centrifugal force inevitably worked on the flowing liquid to destabilize it. The experiments using water as the liquid flowing along a single

helical channel formed by a pair of rubber strings winding around each of the PMMA cylinders placed in an upward flow of CO_2 gas showed a significant promotion of the gas absorption into the water flow as a result of its oscillatory motion induced by the centrifugal force. On the contrary, the water rivulets flowing along such helical channels tended to be thicker than ordinary water films flowing down vertical plain walls, which adversely affected the gas absorption. Based on the results of these single-channel flow experiments, we estimated the performance of the gas-absorption columns each equipped with multiple helical channels. This estimation indicated that an advantage of such helical-channel columns over conventional wetted-wall columns is available when the water flow along the helical channels with a relatively low tilt angle ($\sim 30-45^\circ$ from the horizontal) is accompanied by a centrifugal-force-driven oscillatory motion. Presumably, the gas-absorption performance of helical-channel columns will be improved by optimizing the cross-sectional geometry and the surface wettability of the channel-forming strings or ridges for increasing the spatial proportion of the wetted area on the column wall and thinning the water rivulets flowing along the channels.

Literature Cited

1. Mahr B, Mewes D. Two-phase flow in structured packings: modeling and calculation on a macroscopic scale. *AIChE J*. 2008;54:614–626.
2. INTALOX® Structured Packing, a document prepared by Koch-Glitsch, LP, Wichita, KS. 2010. Bulletin KGSP-1. Rev. 3-2010. Available at: http://www.koch-glitsch.com/Document%20Library/KGSP.pdf (accessed 9 February 2013).
3. Migita H, Soga K, Mori YH. Gas absorption in a wetted-wire column. *AIChE J*. 2005;51:2190–2198.
4. Pakdehi SG, Taheri S. Separation of hydrazine from air by wetted wire column. *Chem Eng Technol*. 2010;33:1687–1694.
5. Broniarz-Press L. Enhancement of mass transfer coefficients in spiral films. *Int J Heat Mass Transfer*. 1997;40:4197–4208.
6. Hijikata K, Nagasaki T, Fukushima D, Kasai K, Sakai M. CO_2 absorption into liquid. *Therm Sci Eng*. 1996;4:65–73.
7. Yoshimura PN, Nosoko T, Nagata T. Enhancement of mass transfer into a falling laminar liquid film by two-dimensional surface waves—some experimental observations and modeling. *Chem Eng Sci*. 1996;51:1231–1240.
8. Park CD, Nosoko T. Three-dimensional wave dynamics on a falling film and associated mass transfer. *AIChE J*. 2003;49:2715–2727.
9. Lide DR, Frederikse HPR. CRC Handbook of Chemistry and Physics, 76th ed. Boca Raton, FL: CRC Press, 1995.
10. Levich VG. Physicochemical Hydrodynamics. Englewood Cliffs, NJ: Prentice-Hall, Inc., 1962:689.
11. Bird RB, Stewart WE, Lightfoot EN. Transport Phenomena, 2nd ed. New York: Wiley, 2002:46.
12. Alekseenko SV, Nakoryakov VE, Pokusaev BG. Wave Flow of Liquid Films. New York: Begell House, Inc., 1994:45–47.
13. Bird RB, Stewart WE, Lightfoot EN. Transport Phenomena, 2nd ed. New York: Wiley, 2002:42–45.
14. Feind K. Strömungsuntersuchungen bei Rieselfilmen. *VDI-Forschungsheft*. 1960;481:5–35.
15. Yih SM, Chen KY. Gas absorption into wavy and turbulent falling liquid films in a wetted-wall column. *Chem Eng Commun*. 1982;17:123–136.
16. Lemmon EW, Huber ML, McLinden M. NIST Reference Fluid Thermodynamic and Transport Properties – REFPROP (ver. 8.0). Gaithersburg, MD: National Institute of Standards and Technology, 2007.
17. Versteeg GF, Swaaij WPM. Solubility and diffusivity of acid gases (CO_2, N_2O) in aqueous alkanolamine solutions. *J Chem Eng Data*. 1988;33:29–34.

Appendix A

Deriving an expression of average mass-transfer coefficient for a helical channel

Let an s axis be laid on the center line of a helical channel such that its origin is located at the elevation of the top end of the effective gas−liquid contact section. The mass conservation of CO_2 dissolved in water flowing through the channel may be written in a differential form as follows

$$\dot{V}dC = Wk_L(C_{sat} - C)ds \tag{A1}$$

where C is the mixed-mean mass concentration of CO_2 dissolved in water at each s-axial location, and k_L is the local liquid-side mass-transfer coefficient. Neglecting any change in $\dot{V}$ due to CO_2 absorption into the flowing water, we can integrate Eq. A1 from the inlet of the gas−liquid contact section, $s = 0$, to its exit, $s = L$, as follows

$$-\int_{C_{top}}^{C_{bot}} \frac{dC}{C - C_{sat}} = \frac{W}{\dot{V}}\int_0^L k_L ds \tag{A2}$$

Noting such a relation between k_L and $\bar{k}_L$ that

$$\frac{1}{L}\int_0^L k_L ds = \bar{k}_L \tag{A3}$$

we can rewrite Eq. A2 as follows

$$-\int_{C_{top}}^{C_{bot}} \frac{dC}{C - C_{sat}} = \frac{WL\bar{k}_L}{\dot{V}} \tag{A4}$$

Carrying out the definite integration on the left-hand side of Eq. A4, we obtain

$$-ln\left(\frac{C_{sat} - C_{bot}}{C_{sat} - C_{top}}\right) = ln\left(\frac{C_{sat} - C_{top}}{C_{sat} - C_{bot}}\right) = \frac{WL\bar{k}_L}{\dot{V}} \tag{A5}$$

which can be readily rewritten into the form of Eq. 5.

Appendix B

Calculating mean transit time for a wetted-wall column

For a 2-D liquid-film flow, the Reynolds number defined by Eq. 5 can be rewritten as follows

$$Re_f = \frac{4\bar{u}\delta}{\nu} \tag{B1}$$

where δ and $\bar{u}$ denote the film thickness and the average flow velocity over a cross section of the film, respectively. As long as the film slowly flows down a vertical wall accompanied by no wave motion, the equation of motion for the flow can be solved to give the following relation between $\bar{u}$ and δ[12,13]

$$\bar{u} = \frac{g\delta^2}{3\nu} \tag{B2}$$

where g denotes the acceleration due to gravity. Combining Eqs. B1 and B2, we obtain the following expression for δ

$$\delta = \left(\frac{3\nu^2}{4g}\right)^{1/3} Re_f^{1/3} \tag{B3}$$

For turbulent film flows in the range that $Re_f \geq 1600$, Feind[14] proposed the following expression for δ

$$\delta = 0.369\left(\frac{3\nu^2}{g}\right)^{1/3}\left(\frac{Re_f}{4}\right)^{1/2} \quad \text{(B4)}$$

Substituting Eq. B3 or B4 into Eq. B1 to eliminate δ, we can calculate $\bar{u}$ as a function of Re_f and determine how $\tau(=H/\bar{u})$, the mean transit time for the film-forming liquid falling down a given height H, varies depending on Re_f. For drawing the δ vs. Re_f and the τ vs. Re_f curves for an 80-cm height wetted-wall column in Figures 7 and 8, we used Eq. B3 for the Re_f range up to 1600 and Eq. B4 for the higher Re_f range above 1600.

Appendix C

Mass-transfer coefficient and absorption efficiency for a wetted-wall column

The gas-absorption performance of an 80-cm height wetted-wall column shown in Figures 9 and 10 was estimated using the correlations for the liquid-side mass-transfer coefficient $\bar{k}_L$ that Yih and Chen[15] prepared based on their experiments of CO_2 absorption into water films falling down the outside surface of a vertical cylinder. The Schmidt number included in the correlations was evaluated to be 463.7 (at 298.15 K and 0.10133 MPa), based on the ν and D_{CO_2} (CO_2-in-water diffusivity) values given by REFPROP[16] and Versteeg and Swaaij,[17] respectively. The absorption efficiency E of this column was deduced from $\bar{k}_L$ via a simple formulation based on the mass conservation of CO_2, which is described below.

Let a downward-directed vertical axis, z, be laid on the wetted-wall such that its origin is located at the elevation of the top end of the effective gas−liquid contact section. If the two-phase system in this section is in a steady state, the mass conservation of CO_2 dissolved in the liquid falling down the column wall may be written in a differential form as follows

$$\langle \dot{V} \rangle dC = k_L(C_{sat} - C)dz \quad \text{(C1)}$$

where $\langle \dot{V} \rangle$ is the volumetric liquid flow rate per unit width of the column wall, C is the mixed-mean mass concentration of CO_2 dissolved in the liquid as a z-dependent variable, and k_L is the local liquid-side mass-transfer coefficient. As $\langle \dot{V} \rangle$ and C_{sat} are invariable with z, Eq. C1 can be integrated from the top, $z = 0$, to the bottom, $z = H$ (=80 cm), of the gas−liquid contact section as follows

$$-\int_{C_{top}}^{C_{bot}} \frac{dC}{C - C_{sat}} = \frac{1}{\langle \dot{V} \rangle}\int_0^H k_L dz \quad \text{(C2)}$$

Noting such a relation between k_L and $\bar{k}_L$ that

$$\frac{1}{H}\int_0^H k_L dz = \bar{k}_L \quad \text{(C3)}$$

we can rewrite Eq. C2 as follows

$$-\int_{C_{top}}^{C_{bot}} \frac{dC}{C - C_{sat}} = \frac{\bar{k}_L H}{\langle \dot{V} \rangle} \quad \text{(C4)}$$

Carrying out the definite integration on the left-hand side of Eq. C4, we obtain

$$ln\left(\frac{C_{sat} - C_{bot}}{C_{sat} - C_{top}}\right) = -\frac{\bar{k}_L H}{\langle \dot{V} \rangle} \quad \text{(C5)}$$

or

$$\frac{C_{sat} - C_{bot}}{C_{sat} - C_{top}} = \exp\left(-\frac{\bar{k}_L H}{\langle \dot{V} \rangle}\right) \quad \text{(C6)}$$

Noting that

$$\frac{C_{sat} - C_{bot}}{C_{sat} - C_{top}} = 1 - \frac{C_{bot} - C_{tot}}{C_{sat} - C_{top}} = 1 - E \quad \text{(C7)}$$

and

$$\langle \dot{V} \rangle = \bar{u}\delta = \frac{\nu Re_f}{4} \quad \text{(C8)}$$

Eq. C6 can be rewritten as follows

$$E = 1 - \exp\left(-\frac{4\bar{k}_L H}{\nu Re_f}\right) \quad \text{(C9)}$$

This expression was used to determine the E vs. Re_f relation for the wetted-wall column plotted in Figure 10.

The $\bar{k}_L$ vs. $\dot{V}$ and E vs. $\dot{V}$ relations for an 80-cm height wetted-wall column having a specified diameter, $D = 40$ or 60 mm, plotted in Figure 11 were calculated by replacing Re_f in Yih and Chen's correlations for $\bar{k}_L$ and Eq. C9 by $(4\dot{V})/(\pi D\nu)$.

Manuscript received Dec. 31, 2012, and revision received Feb. 15, 2013.